

Single-shot quantum measurements sketch quantum states

Jia-Bao Wang and Yi Zhang*

*International Center for Quantum Materials, Peking University, Beijing, 100871, China and
School of Physics, Peking University, Beijing, 100871, China*

Quantum measurements are our eyes to the quantum systems consisting of a multitude of microscopic degrees of freedom. However, the intrinsic uncertainty of quantum measurements and the exponentially large Hilbert space pose natural barriers to simple interpretations of the measurement outcomes. We propose a nonlinear “measurement energy” based upon the measurement outcomes and an iterative effective-Hamiltonian approach to extract the most probable states (maximum likelihood estimates) in an efficient and general fashion, thus reconciling the non-commuting observables and getting more out of the quantum measurements. We showcase the versatility and accuracy of our perspective on random long-range fermion models and Kitaev quantum spin liquid models, where smoking-gun signatures were lacking. Our study also paves the way towards concepts such as nonlinear-operator Hamiltonian and applications such as parent Hamiltonian reconstruction.

Introduction —Quantum systems exhibit fascinating and elusive quantum phenomena, such as quantum fluctuations, strong correlations [1], quantum entanglements [2–9], quantum anomalies [10–15], with no counterpart in the macroscopic world [16]. Nontrivial spin and electronic systems like quantum spin liquid (QSL) [17–20], superconductors [21–24], topological phases [11, 12, 25–33], form a cornerstone of modern-day science and technology. While scientists have made much progress and established physical pictures that are both simple and beautiful, it is common that we scratch our heads over their complex behaviors when encountering the vast and intertwined charges, spins, lattices, etc., microscopic or emergent degrees of freedom [34, 35].

Experiments on quantum systems are our window to their microscopic world. However, analysis on quantum measurements is intrinsically difficult since the principles of quantum mechanics induce fluctuations that whenever a general observable $\hat{O} = \sum_{\gamma} a_{\gamma} \hat{P}_{\gamma}$ is measured, the outcome inevitably and stochastically picks one of the a_{γ} eigenvalues with probability $\langle \hat{P}_{\gamma} \rangle$ [36]. Fortunately, if we measure the same target state repeatedly, through either identical copies or relaxation, the resulting average suppresses the fluctuations and converges to the expectation value $\langle \hat{O} \rangle$, which is non-stochastic [36] and often more physically meaningful. The investigation may be further facilitated with a phenomenological picture or microscopic model, whose predictions offer smoking-gun signatures that we can look for and compare with the quantum measurements. However, such a strategy may also incur potential limitations: by presuming a model or picture, we not only waste the seemingly unrelated data but also risk carrying biases consciously or unconsciously. In addition, exotic quantum matters such as QSLs lack definitive signatures, compelling scientists to resort to a negative-evidence stance [19, 37] that remains controversial and less controlled to a degree.

In this letter, we discuss an alternative and general strategy to determine the most probable quantum states given the raw quantum measurement data. We inter-

pret the quantum measurements as nonlinear measurement energy and offer an iterative effective-Hamiltonian strategy to obtain the minimums in the Hilbert space and thus locate the maximum likelihood estimate (MLE) quantum states. Once we attain the target states, we have all its information at disposal, including ones not directly achievable from quantum measurements, such as quantum entanglements [2–9] and certain topological characters [7–11]. In this way, we can utilize all measurement outcomes on a neutral and equal footing and remove the necessity of a presumed model or picture that may cause potential bias. We showcase the strategy’s generality and effectiveness on random long-range fermion models and Kitaev spin liquid [18], neither of which has any smoking-gun signature that can compare with the quantum measurements. The more quantum measurements we make, the more information we have, and the more accurately we can locate the quantum states. Even a single-shot quantum measurement matters, as its outcome provides information, and we illustrate a successful case where the quantum measurements consist of nothing but the single shots. Quantum state tomography, which aims to reconstruct the quantum state through quantum measurements has been a long-standing topic in quantum physics [38]. The recent introduction of neural-network-based tomography [39, 40] and shadow tomography [41] have achieved practical efficiency over multiple qubits. However, the neural networks are approximate, and the shadow tomography requires random tractable unitaries before quantum measurements that can be hard to implement. Our strategy does not need such compromises.

The measurement energy —Consider the a-priori probability distribution $w(\Phi)$ of all quantum states $|\Phi\rangle$ spanning the Hilbert space, if a single-shot measurement of observable $\hat{O} = \sum_{\gamma} a_{\gamma} \hat{P}_{\gamma}$ yields an outcome $a_{\gamma'}$, the posterior probability after this measurement is:

$$w(\Phi) \rightarrow p(\Phi|\gamma') = p(\gamma'|\Phi)w(\Phi)/p(\gamma'), \quad (1)$$

following the Bayesian formula. Here, a_{γ} and \hat{P}_{γ} are the eigenvalues and the corresponding projection operators of

the observable \hat{O} , $p(\gamma'|\Phi) = \langle \Phi | \hat{P}_{\gamma'} | \Phi \rangle$ is the probability of outcome $a_{\gamma'}$ given the quantum state $|\Phi\rangle$, and $p(\gamma')$ offers normalization [42].

As the experiment progresses, we obtain a series of results $\mathcal{D} = \{\gamma_1, \gamma_2, \dots\}$ of single-shot measurements over observables $\{\hat{O}_1, \hat{O}_2, \dots\}$, and update the probability as:

$$w(\Phi) \propto \prod_{\gamma \in \mathcal{D}} p(\gamma|\Phi) = \prod_{\gamma \in \mathcal{D}} \langle \Phi | \hat{P}_{\gamma} | \Phi \rangle. \quad (2)$$

We define the ‘‘measurement energy’’:

$$E(\Phi) = - \sum_{\gamma \in \mathcal{D}} \log \langle \Phi | \hat{P}_{\gamma} | \Phi \rangle = - \sum_{\gamma \in \mathcal{R}} N_{\gamma} \log \langle \Phi | \hat{P}_{\gamma} | \Phi \rangle, \quad (3)$$

so that $w(\Phi) \propto \exp[-E(\Phi)]$ of a quantum state $|\Phi\rangle$ becomes analogous to the Boltzmann distribution with energy $E(\Phi)$ in unit of $k_B T$. We note that unlike the energy expectation value of a conventional Hamiltonian of linear operators, the measurement energy here is explicitly nonlinear due to the log function. Therefore, the probability distribution of a quantum state with quantum-measurement outcomes offers realizations of exotic nonlinear-operator Hamiltonian.

In the last step of Eq. 3, we have binned together single-shot measurements with the same $\hat{O} \rightarrow a_{\gamma}$, with N_{γ} instances each. The result, further re-expressed as $E(\Phi) = - \sum_{\gamma \in \mathcal{R}} N_{\hat{O}} f_{\gamma} \log \langle \Phi | \hat{P}_{\gamma} | \Phi \rangle$, clearly describes the measurement energy as the cross entropy between the expected probability given a quantum state $|\Psi\rangle$ and the measured probability $f_{\gamma} = N_{\gamma}/N_{\hat{O}}$, further weighted by the number of measurements $N_{\hat{O}}$ on each observable \hat{O} . Next, We develop a simple protocol using self-consistent effective Hamiltonians to locate the measurement-energy minimums in the Hilbert space for the most probable quantum states.

Measurement-energy minimums via iterative effective Hamiltonians —For a generic nonlinear cost function $E = f(\langle \hat{O} \rangle)$ defined for the expectation values $\langle \hat{O}_i \rangle = \langle \Phi | \hat{O}_i | \Phi \rangle$, its functional derivative with respect to $|\Phi\rangle$ should vanish at the minimum:

$$\delta E = \sum_i \left. \frac{\partial f(\langle \hat{O} \rangle)}{\partial \langle \hat{O}_i \rangle} \right|_{\langle \hat{O} \rangle_0} \cdot \delta \langle \hat{O}_i \rangle_0 = 0, \quad (4)$$

where $\langle \hat{O}_i \rangle_0$ are the expectation values at the minimum. Commonly, this is a difficult problem; however, we note that a Hamiltonian \hat{H}_{eff} on the same Hilbert space and consisting of the same linear operators:

$$\hat{H}_{eff} = \sum_i \alpha_i \hat{O}_i, \quad (5)$$

should possess a ground state $|\Phi'_0\rangle$ that satisfies $\delta \langle \hat{H}_{eff} \rangle = \sum_i \alpha_i \cdot \delta \langle \hat{O}_i \rangle_0 = 0$, which coincide with Eq. 4 if we set $|\Phi'_0\rangle = |\Phi_0\rangle$ and:

$$\alpha_i = \left. \frac{\partial f(\langle \hat{O} \rangle)}{\partial \langle \hat{O}_i \rangle} \right|_{\langle \hat{O} \rangle_0}. \quad (6)$$

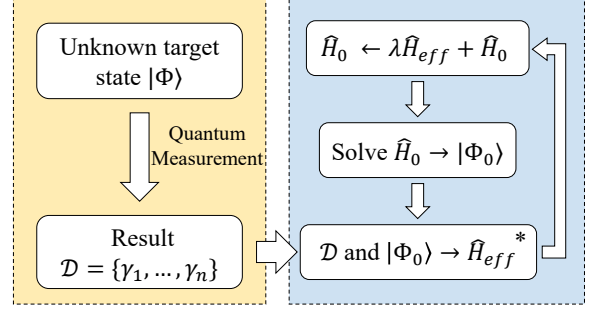


FIG. 1. We outline our strategy for the MLE quantum state: given the quantum measurement results, we iteratively solve \hat{H}_0 for the state $|\Phi_0\rangle$ and update \hat{H}_0 with \hat{H}_{eff} following* Eq. 7.

Eqs. 5 and 6 can be solved self-consistently.

Applying such protocol to the measurement energy in Eq. 3, the effective Hamiltonian is:

$$\hat{H}_{eff} = \sum_{\gamma \in \mathcal{R}} \alpha_{\gamma} \hat{P}_{\gamma}, \quad (7)$$

where $\alpha_{\gamma} = -N_{\gamma}/\langle \Phi_0 | \hat{P}_{\gamma} | \Phi_0 \rangle$. This is one of the main conclusions of the letter. Note that different observables may contribute to the same projection operator. The self-consistent ground state $|\Phi_0\rangle$ of Eq. 7 is our MLE quantum state given the quantum measurements. In practice, we obtain $|\Phi_0\rangle$ as the ground state of \hat{H}_0 (instead of H_{eff}) in each iteration and update $\hat{H}_0 \rightarrow \hat{H}_0 + \lambda \hat{H}_{eff}$ for stability and precision, where λ is a rate-controlling parameter. We summarize the strategy, partially inspired by the optimization in supervised machine learning [43–46], in Fig. 1.

To see the effect of this setup, let’s consider the target state of a spin-1/2 spinor $|\Phi\rangle = \cos(\theta/2)|\uparrow\rangle + \sin(\theta/2)\exp(i\varphi)|\downarrow\rangle$ as a toy-model example. After a sufficient number M of quantum measurements of $\hat{S}_z = \hbar\sigma^z/2$, the outcomes behave as:

$$\lim_{M \rightarrow \infty} M_{\pm} = M \langle \Phi_0 | \hat{P}_{\pm} | \Phi_0 \rangle = M \frac{(1 \pm \cos \theta)}{2}, \quad (8)$$

where $\hat{P}_{\pm} = (1 \pm \sigma^z)/2$ are the projection operators onto the $\sigma^z = \pm 1$ eigenspaces, respectively. For an iteration state current at $|\Phi_0\rangle = \cos(\theta'/2)|\uparrow\rangle + \sin(\theta'/2)\exp(i\varphi')|\downarrow\rangle$, $\alpha_{\pm} = -M(1 \pm \cos \theta)/(1 \pm \cos \theta')$ contributes the following terms to the next \hat{H}_{eff} :

$$\alpha_+ \hat{P}_+ + \alpha_- \hat{P}_- = -M \frac{\cos \theta - \cos \theta'}{1 - \cos^2 \theta'} \sigma^z + const. \quad (9)$$

It is straightforward to see that when $\theta' > \theta$ ($\theta' < \theta$), the coefficient of σ^z is negative (positive), giving preference to a smaller (larger) θ' for the next iteration, and so on so forth toward the target state. We also note that the \hat{S}_z

measurements provide no information on φ . Therefore, φ' remains its initial value unless there are measurements on observables that depend on φ , such as \hat{S}_x and \hat{S}_y .

However, there is a potential problem: as the iteration state approaches the target state, $\langle \Phi | \hat{P}_\gamma | \Phi \rangle$ approaches f_γ , \hat{H}_{eff} grows small, and its eigenstates become unstable to noises and fluctuations. For example, Eq. 9 vanishes (upto a trivial constant) when $\theta' \rightarrow \theta$. Therefore, we would rather use \hat{H}_{eff} as a gradient to update the iteration model $\hat{H}_0 \rightarrow \hat{H}_0 + \lambda \hat{H}_{eff}$ for the better - a gradient descent of a quantum Hamiltonian. Similar to supervised machine learning [43–46], the gradient-descent rate λ plays an important role in the performance at convergence, which we discuss in further details in Supplemental Materials.

Example: random long-range fermion model—Let's consider the ground state of the following Hamiltonian:

$$\hat{H} = - \sum_{ij} t_{ij} (c_i^\dagger c_j + c_j^\dagger c_i) - \sum_i \mu_i c_i^\dagger c_i, \quad (10)$$

where $1 \leq i, j \leq L$. We apply random $t_{ij} \in [0, 1]$ between arbitrary sites and $\mu_i \in [-0.5, 0.5]$ to deny the system symmetries and locality. Still, our strategy can derive the target states, placed in a black box and tangible only via quantum measurements, even on relatively large systems.

It is high time we discussed the choices of observables \hat{O} . On the one hand, \hat{O} is strongly limited by the quantum measurements, e.g., quantum systems and apparatus; on the other hand, \hat{O} plays an essential yet implicit role in our story, as it determines the projection operators \hat{P}_γ in Eq. 7. We note that an observable with more eigenvalues, e.g., $c_x^\dagger c_y + c_y^\dagger c_x$ with three eigenvalues: $\{0, \pm 1\}$, acts as a double-edge sword: they may incur cost and difficulty in post-processing \hat{H}_{eff} due to more complex \hat{P}_γ , but also offer more information than the expectation value - a distribution carries more information than the average alone, in similar spirit to shot-noise studies [47, 48]. On the contrary, when we choose $\hat{O}_x = c_x^\dagger c_x$ and $\hat{O}_{xy} = (c_x^\dagger + c_y^\dagger)(c_x + c_y)/2$ with eigenvalues $\{0, 1\}$, \hat{P}_γ and \hat{H}_{eff} remain fermion-bilinear, and $|\Phi_0\rangle$ can be obtained straightforwardly at each iteration.

Let's say we measure each observable $\hat{O} = \sum_\gamma \alpha_\gamma \hat{P}_\gamma$ $N_{\hat{O}} = M$ times on the target quantum state with M_γ outcomes of α_γ respectively. For benchmark, we first consider the $M \rightarrow \infty$ limit with fully suppressed fluctuations, so that $M_\gamma \rightarrow M \times \langle P_\gamma \rangle$. Putting these results from $L = 100$ systems into the iterative process in Eq. 7, we summarize the results in Fig. 2. We observe a quick convergence of the iteration state $|\Phi_0\rangle$ towards the target state, as well as its average measurement energy $E(|\Phi_0\rangle)$ towards its lower bound $\min(E) = -\sum_{\gamma \in \mathcal{R}} N_{\hat{O}} f_\gamma \log f_\gamma$. The infidelity spikes when an iteration state $|\Phi_0\rangle$ messes up its particle number over the slight modifications.

The strategy also works for data laden with quantum fluctuations from a finite number of quantum measure-

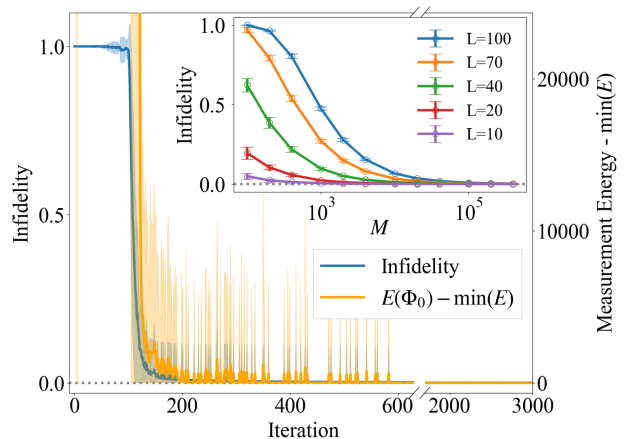


FIG. 2. Quickly in our iterations, the iteration state $|\Phi_0\rangle$ converges to the target quantum state (infidelity $\sim 6 \times 10^{-4}$), and the average measurement energy $E(|\Phi_0\rangle)$ converges to its lower bound. The system size is $L = 100$. The inset shows the obtained quantum states' increasingly better convergence to the target states after 1000 iterations when we include more measurements, characterized by M , for different system sizes. The shade and error bars are based upon 100 trials on different target states.

ments and when the number of measurements differs between observables. More generally, we can measure \hat{O}_x and \hat{O}_{xy} observables on a generic quantum many-body state, although this will constrain the iteration state $|\Phi_0\rangle$ to a search space of Hartree-Fock states away from the target state, characterized by the extent of measurement energy above its lower bound. We summarize these results in the inset of Fig. 2, and further in Supplemental Materials. More throughout analysis requires additional observables capable of capturing interactions and leading to a more generic \hat{H}_{eff} , where we shall need numerical methods such as exact diagonalization (ED), density-matrix renormalization group (DMRG) [49, 50], and quantum Monte Carlo methods [51, 52].

Example: strongly-correlated Kitaev QSL state—Let's consider the nearest-neighbor spin Hamiltonian on the honeycomb lattice:

$$\hat{H} = \sum_{\langle ij \rangle \in \alpha\beta(\gamma)} \left[J \vec{S}_i \cdot \vec{S}_j + K S_i^\gamma S_j^\gamma + \Gamma \left(S_i^\alpha S_j^\beta + S_i^\beta S_j^\alpha \right) \right], \quad (11)$$

which is a good description of the Kitaev physics in the A_2IrO_3 -family iridates [53] and Kitaev material $RuCl_3$ [20]. K , J , and Γ are the amplitudes of the Kitaev interaction, isotropic Heisenberg interaction, and the symmetric off-diagonal interactions, respectively. Depending on the bond dimension, each bond is labeled by $\alpha\beta(\gamma)$, where $\gamma = x, y, z$ is the spin direction in the Kitaev term, and α, β are the two orthogonal spin directions in the Γ term. We take the ground state of \hat{H} with a dominant Kitaev term on a 3×3 system with periodic boundary condition, illustrated in Fig. 3, as our target quantum

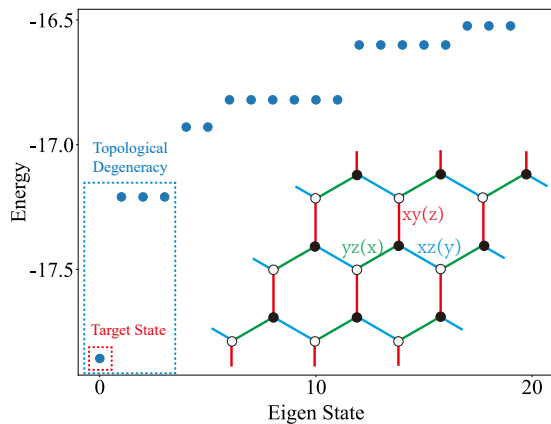


FIG. 3. The spectra and sketch of the Kitaev model in Eq. 11 on a honeycomb lattice consists of spin interactions depending on the bond directions, labeled by different colors. The system size is 3×3 with periodic boundary conditions. The spectra is for $K = 1$, $J = 0.1$, and $\Gamma = 0$.

state.

The pristine Kitaev model ($J = \Gamma = 0$) is analytically solvable with QSL ground states. QSL has received much recent interest due to its exotic quantum origin, topological nature and excitations, and potential connection to unconventional superconductivity. However, there have been difficulty and controversy in establishing QSL within candidate quantum materials due to a lack of smoking-gun signatures. Instead, we assume our strategy and probe the target quantum states with seemingly trivial quantum measurements. As we will see, these measurements provide helpful information and lead us to the target state and, in turn, its abstract natures including QSL phase [7–9] and quantum entanglements [2–6].

To begin with, we set $J = 0.1$, $K = 1$. Due to the finite-site effect, a small splitting appears between the four topologically degenerate ground states, shown in Fig. 3. For quantum measurements on $\sigma_i^\lambda \sigma_j^\lambda$ of each $\langle ij \rangle$ bond on the lowest energy state, $\lambda = x, y, z$, we obtain $M_\pm(ij, \lambda) = M \times \langle \hat{P}_\pm(ij, \lambda) \rangle$ counts of ± 1 outcomes, respectively, in the large $M \rightarrow \infty$ limit. $\hat{P}_\pm(ij, \lambda) = (1 \pm \sigma_i^\lambda \sigma_j^\lambda)/2$. Similar quantum measurements are potentially available to QSL models in Rydberg-atom systems [54, 55], or via electron spin resonance scanning tunneling microscopy experiments [56, 57], etc. Putting these results into the iterations in Eq. 7, $|\Phi_0\rangle$ successfully converges to the target state, see the inset of Fig. 4. Interestingly, through measurements on a single ground state, we also obtain the other three topologically degenerate states as a by-product, and the overall manifold shows high fidelity with that of the target model; see Supplemental Materials for more details on the ground-state degeneracy [18, 29, 58]. On the one hand, these degenerate states share similar local properties and are indeed equally qualified for the MLE states; on the other hand,

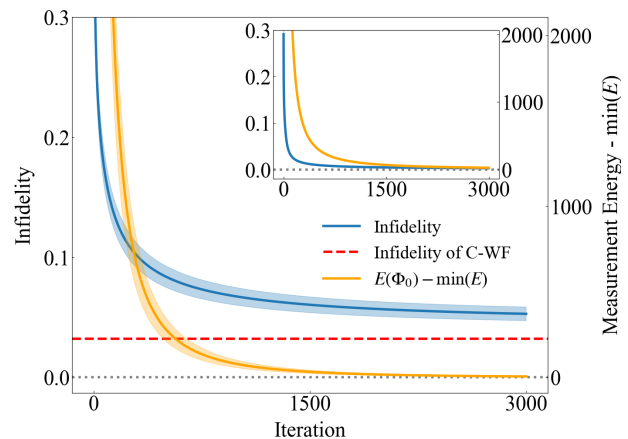


FIG. 4. With the measurement results on the ground state of Eq. 11 (spectrum shown in Fig. 3), the measurement energy $E(\Phi_0)$ quickly saturates the lower bound, while the iteration states $|\Phi_{0;trial}\rangle$ at the convergence show slight infidelity $\sim 5 \times 10^{-2}$ with the target state and visibly differ from each other between different trials. Here, $K = 1$, $J = 0.1$, and $\Gamma \in [0, 0.1]$. Inset: in comparison, for the same quantum measurements yet on the ground state with $\Gamma = 0$, not only the measurement energy $E(\Phi_0)$ converges to the lower bound, the iteration state $|\Phi_0\rangle$ converges quickly and uniquely to the target state as well. The shade is the span over 10 trials with different initialization.

the simultaneous presence of topological degeneracy implies that \hat{H}_0 has inherited the topological information that must have been present in the target ground state [7–9].

Another interesting scenario is when the observables involved are insufficient to distinguish the target state, as there are multiple states that saturate the measurement energy to the lower bound, e.g., the spinor states with the target θ yet arbitrary ϕ given only \hat{S}_z measurements. For this intention, we carry over the same setup, namely, $\sigma_i^\lambda \sigma_j^\lambda$, $\lambda = x, y, z$, and a large number $M \rightarrow \infty$ of quantum measurements, over more complicated ground states with $J = 0.1$, $K = 1$ as before but an additional, random $\Gamma \in [0, 0.1]$ on each bond [59]. Given such data, the iterations of 10 independent trials with different initial H_0 are summarized in Fig. 4. While all trials converge fully and leave little measurement-energy residue above the lower bound, the obtained MLE states $|\Phi_{0;trial}\rangle$ differ from trial to trial, with an overlap ~ 0.90 . Unfortunately, as all of these states satisfy the available information similarly, we cannot tell which state is closer to the target state and how close it is. It calls for additional observables that can bring new information or, when ambiguity is not overwhelming, a common ground between $|\Phi_{0;trial}\rangle$ as a contingency plan, detailed in Supplemental Materials. As before, the states topologically degenerate to the target state also emerge.

Finally, we consider an unprecedented scenario to showcase the adaptability of our strategy. We choose

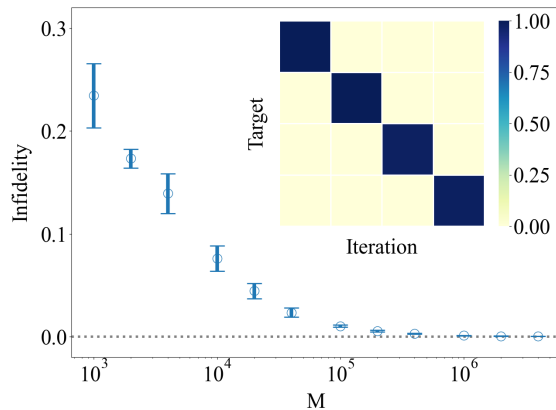


FIG. 5. Single-shot quantum measurements $\sigma_i^{\hat{n}}\sigma_j^{\hat{n}}$ for \hat{n} along random solid angles are laden with randomness and fluctuations. Our perspective, however, allows a derivation of the MLE states $|\Phi_0\rangle$ based upon such single-shot outcomes, which converge before 1500 iterations and are asymptotically consistent with the target states as the number of measurements M increases. The target states are similar to those in Fig. 4, and the error bars are based upon 10 different trials. The inset demonstrates the fidelity between the lowest four eigenstates of the iteration \hat{H}_0 at convergence and the topological degeneracy of the target system.

the $\sigma_i^{\hat{n}}\sigma_j^{\hat{n}}$ on nearest-neighbor bonds for \hat{n} along random solid-angle directions, $\sigma_i^{\hat{n}} = \vec{n} \cdot \vec{\sigma}_i$, different from time to time. Each observable is measured only once, yielding a single outcome of ± 1 according to the quantum probability. Such results are intrinsically plagued with such quantum fluctuation and randomness that there is no well-defined statistics to speak of. However, we can capitalize the information from such single-shot measurements to unravel the underlying target state. We summarize the results of this paramount demonstration in Fig. 5. Note that a measurement-energy lower bound is no longer available for such single-shot outcomes. The more single shots (M is the number of single shots per bond), the more information at disposal, and the higher the fidelity of the MLE state $|\Phi_0\rangle$ to the target states. We note that although our setup of random measurements resembles the shadow tomography [60], it does not satisfy the prerequisite randomness of the latter. Indeed, our strategy is more generally applicable and does not rely on the randomness, or any other scheme, of the measurements.

Discussions —In addition to our “gradient descent” approach on the effective Hamiltonian, the maximum likelihood estimates of Eq. 3 may also be obtainable via numerical methods such as DMRG [49, 50], where variational quantum states are optimized with respect to a cost function. On the other hand, the chosen variational ansatz may constrain the search, e.g., the matrix product states cannot capture the random long-range fermion states due to its locality requirement [61]. In comparison, while our strategy is indeed general, there exist barriers

in handling the effective Hamiltonian when it takes a strongly correlated form. We may also process the iterations using a hybrid algorithm with the help of a quantum simulator [62–64], which evaluates the expectation values for Eq. 7, while a classical computer takes care of the rest.

We emphasize that as we have observed in our examples, the resulting \hat{H}_0 does not necessarily need to connect with the original Hamiltonian harboring the target state, as the mapping between Hamiltonians and eigenstates is many-to-one. Interestingly, such \hat{H}_0 also paves the way for parent Hamiltonian reconstruction [65, 66]. In addition, given different initializations and the gradient descent nature of the search, \hat{H}_0 may differ from trial to trial - a unique advantage of this strategy that allows exploring universality.

Considering the vast 2^L -dimensional Hilbert space of a quantum many-body system, we have offered a quantum strategy to interpret quantum measurements in a general and precise way. We note that the additive form of the measurement energy in Eq. 3 means that *every single-shot quantum measurement counts*. On the other hand, for cases where the frequency of eigenvalues (measurement outcomes) cannot be obtained directly, we can reverse engineer f_γ from the expectation values $\langle \hat{O} \rangle$, $\langle \hat{O}^2 \rangle$, \dots [36], and $M_{\hat{O}}$ serves as a confidence measure. In theory, the strategy can also be generalized to target mixed states represented by density operators. Whether the same thing can be said for quantum measurements connecting ground state and excited states, e.g., inelastic spectroscopy experiments, remains an open question for future research.

Acknowledgement: We acknowledge helpful discussions with Zhen-Duo Wang, Tian-Lun Zhao, Pei-Lin Zheng, Hao-Yan Chen, and Yuan Wan. We also acknowledge support from the National Science Foundation of China (No.12174008). The calculations of this work are supported by HPC facilities at Peking University.

* frankzhangyi@gmail.com

- [1] J. Quintanilla and C. Hooley, *Physics World* **22**, 32 (2009).
- [2] A. Kitaev and J. Preskill, *Phys. Rev. Lett.* **96**, 110404 (2006).
- [3] M. Levin and X.-G. Wen, *Phys. Rev. Lett.* **96**, 110405 (2006).
- [4] X. Chen, Z.-C. Gu, and X.-G. Wen, *Phys. Rev. B* **82**, 155138 (2010).
- [5] Y. Zhang, T. Grover, and A. Vishwanath, *Phys. Rev. B* **84**, 075128 (2011).
- [6] Y. Zhang, T. Grover, and A. Vishwanath, *Phys. Rev. Lett.* **107**, 067202 (2011).
- [7] Y. Zhang, T. Grover, A. Turner, M. Oshikawa, and A. Vishwanath, *Phys. Rev. B* **85**, 235151 (2012).
- [8] T. Grover, Y. Zhang, and A. Vishwanath, *New Journal*

- of Physics **15**, 025002 (2013).
- [9] Y. Zhang, T. Grover, and A. Vishwanath, Phys. Rev. B **91**, 035127 (2015).
- [10] F. D. M. Haldane, Phys. Rev. Lett. **61**, 2015 (1988).
- [11] R. B. Laughlin, Phys. Rev. Lett. **50**, 1395 (1983).
- [12] C. L. Kane and E. J. Mele, Phys. Rev. Lett. **95**, 146802 (2005).
- [13] M. Z. Hasan and C. L. Kane, Rev. Mod. Phys. **82**, 3045 (2010).
- [14] H. Nielsen and M. Ninomiya, Physics Letters B **130**, 389 (1983).
- [15] X. Yuan, C. Zhang, Y. Zhang, Z. Yan, T. Lyu, M. Zhang, Z. Li, C. Song, M. Zhao, P. Leng, M. Ozerov, X. Chen, N. Wang, Y. Shi, H. Yan, and F. Xiu, Nature Communications **11**, 1259 (2020).
- [16] B. Keimer and J. E. Moore, Nature Physics **13**, 1045 (2017).
- [17] A. Kitaev, Annals of Physics **303**, 2 (2003).
- [18] A. Kitaev, Annals of Physics **321**, 2 (2006).
- [19] S. Yan, D. A. Huse, and S. R. White, Science **332**, 1173 (2011).
- [20] A. Banerjee, C. A. Bridges, J.-Q. Yan, A. A. Aczel, L. Li, M. B. Stone, G. E. Granroth, M. D. Lumsden, Y. Yiu, J. Knolle, S. Bhattacharjee, D. L. Kovrizhin, R. Moessner, D. A. Tennant, D. G. Mandrus, and S. E. Nagler, Nature Materials **15**, 733 (2016).
- [21] J. G. Bednorz and K. A. Müller, Zeitschrift für Physik B Condensed Matter **64**, 189 (1986).
- [22] Y. Kamihara, H. Hiramatsu, M. Hirano, R. Kawamura, H. Yanagi, T. Kamiya, and H. Hosono, Journal of the American Chemical Society **128**, 10012 (2006).
- [23] Y. Kamihara, T. Watanabe, M. Hirano, and H. Hosono, Journal of the American Chemical Society **130**, 3296 (2008).
- [24] Y. Cao, V. Fatemi, S. Fang, K. Watanabe, T. Taniguchi, E. Kaxiras, and P. Jarillo-Herrero, Nature **556**, 43 (2018).
- [25] K. v. Klitzing, G. Dorda, and M. Pepper, Phys. Rev. Lett. **45**, 494 (1980).
- [26] D. C. Tsui, H. L. Stormer, and A. C. Gossard, Phys. Rev. Lett. **48**, 1559 (1982).
- [27] F. D. M. Haldane, Phys. Rev. Lett. **50**, 1153 (1983).
- [28] K. von Klitzing, Rev. Mod. Phys. **58**, 519 (1986).
- [29] X. G. Wen and Q. Niu, Phys. Rev. B **41**, 9377 (1990).
- [30] F. D. M. Haldane, Phys. Rev. Lett. **93**, 206602 (2004).
- [31] B. A. Bernevig, T. L. Hughes, and S.-C. Zhang, Science **314**, 1757 (2006).
- [32] L. Fu, C. L. Kane, and E. J. Mele, Phys. Rev. Lett. **98**, 106803 (2007).
- [33] X. Chen, Z.-C. Gu, Z.-X. Liu, and X.-G. Wen, Science **338**, 1604 (2012).
- [34] E. Fradkin, S. A. Kivelson, and J. M. Tranquada, Rev. Mod. Phys. **87**, 457 (2015).
- [35] C. Proust and L. Taillefer, Annual Review of Condensed Matter Physics **10**, 409 (2019).
- [36] J. J. Sakurai and J. Napolitano, *Modern quantum mechanics; 2nd ed.* (Addison-Wesley, San Francisco, CA, 2011).
- [37] T.-H. Han, J. S. Helton, S. Chu, D. G. Nocera, J. A. Rodriguez-Rivera, C. Broholm, and Y. S. Lee, Nature **492**, 406 (2012).
- [38] A. I. Lvovsky and M. G. Raymer, Rev. Mod. Phys. **81**, 299 (2009).
- [39] G. Torlai, G. Mazzola, J. Carrasquilla, M. Troyer, R. Melko, and G. Carleo, Nature Physics **14**, 447 (2018).
- [40] J. Carrasquilla, G. Torlai, R. G. Melko, and L. Aolita, Nat. Mach. Intell. **1**, 155 (2019).
- [41] H.-Y. Huang, R. Kueng, and J. Preskill, Nature Physics **16**, 1050 (2020).
- [42] F. Huszár and N. M. Houlby, Physical Review A **85**, 052120 (2012).
- [43] Michael Nielsen, *Neural Networks and Deep Learning* (Free Online Book, 2013).
- [44] J. Carrasquilla and R. G. Melko, Nature Physics **13**, 431 (2017).
- [45] Y. Zhang and E.-A. Kim, Phys. Rev. Lett. **118**, 216401 (2017).
- [46] Y. Zhang, A. Mesaros, K. Fujita, S. Edkins, M. Hamidian, K. Ch'ng, H. Eisaki, S. Uchida, J. S. Davis, E. Khatami, *et al.*, Nature **570**, 484 (2019).
- [47] P. Zhou, L. Chen, Y. Liu, I. Sochnikov, A. T. Bollinger, M.-G. Han, Y. Zhu, X. He, I. Bozovic, and D. Natelson, Nature **572**, 493 (2019).
- [48] E. Sivre, H. Duprez, A. Anthore, A. Aassime, F. D. Parmentier, A. Cavanna, A. Ouerghi, U. Gennser, and F. Pierre, Nature Communications **10**, 5638 (2019).
- [49] M. Fannes, B. Nachtergaele, and R. F. Werner, Communications in Mathematical Physics **144**, 443 (1992).
- [50] U. Schollwöck, Rev. Mod. Phys. **77**, 259 (2005).
- [51] W. M. C. Foulkes, L. Mitas, R. J. Needs, and G. Rajagopal, Rev. Mod. Phys. **73**, 33 (2001).
- [52] M. Troyer and U.-J. Wiese, Phys. Rev. Lett. **94**, 170201 (2005).
- [53] J. G. Rau, E. K.-H. Lee, and H.-Y. Kee, Phys. Rev. Lett. **112**, 077204 (2014).
- [54] R. Verresen, M. D. Lukin, and A. Vishwanath, Phys. Rev. X **11**, 031005 (2021).
- [55] G. Semeghini, H. Levine, A. Keesling, S. Ebadi, T. T. Wang, D. Bluvstein, R. Verresen, H. Pichler, M. Kalinowski, R. Samajdar, A. Omran, S. Sachdev, A. Vishwanath, M. Greiner, V. Vuletić, and M. D. Lukin, Science **374**, 1242 (2021).
- [56] A. V. Balatsky, M. Nishijima, and Y. Manassen, Advances in Physics **61**, 117 (2012).
- [57] M. Ternes, New Journal of Physics **17**, 063016 (2015).
- [58] M. B. Hastings and X.-G. Wen, Phys. Rev. B **72**, 045141 (2005).
- [59] The Γ terms are beyond the operator pool descending from the observables.
- [60] H.-Y. Huang, R. Kueng, and J. Preskill, Nature Physics **16**, 1050 (2020).
- [61] U. Schollwöck, Annals of Physics **326**, 96 (2011).
- [62] E. Farhi, J. Goldstone, and S. Gutmann, "A quantum approximate optimization algorithm," (2014), arXiv:1411.4028 [quant-ph].
- [63] L. Zhou, S.-T. Wang, S. Choi, H. Pichler, and M. D. Lukin, Phys. Rev. X **10**, 021067 (2020).
- [64] P. Vikstål, M. Grönkvist, M. Svensson, M. Andersson, G. Johansson, and G. Ferrini, Phys. Rev. Applied **14**, 034009 (2020).
- [65] X.-L. Qi and D. Ranard, Quantum **3**, 159 (2019).
- [66] X. Turkeski, T. Mendes-Santos, G. Giudici, and M. Dalmonde, Phys. Rev. Lett. **122**, 150606 (2019).